

Self-Organization Properties and Microstructures of Sodium *N*-(11-Acrylamidoundecanoyl)-L-valinate and -L-threoninate in Water

Sumita Roy and Joykrishna Dey*

Department of Chemistry, Indian Institute of Technology, Kharagpur –721 302, India

Received April 25, 2005; E-mail: joydey@chem.iitkgp.ernet.in

A new class of *N*-acylamino acid surfactants, sodium *N*-(11-acrylamidoundecanoyl)-L-valinate (SAUV) and -L-threoninate (SAUT), were synthesized and characterized in aqueous solutions. The self-assembly properties were studied by surface tension, fluorescence probe, light scattering, and microscopic techniques. The interfacial properties of the amphiphiles have been investigated at the air/water interface. The critical aggregation concentration (*cac*) and free energy change of aggregation for both amphiphiles were determined. The results of fluorescence probe and surface tension studies have indicated that initially flat bilayer structures are formed, which upon a further increase of surfactant concentration transform into closed vesicles. The pH and temperature dependence of the bilayer aggregates have been studied. The role of intermolecular hydrogen bonding between amide groups upon aggregation towards microstructure formation in solution has been elucidated. The micropolarity of the hydrophobic domains of the bilayer self-assemblies was estimated by fluorescence probe methods. Dynamic light scattering measurements were performed to determine the mean size of the aggregates. The circular dichroism spectra of SAUV and SAUT suggested the formation of chiral aggregates in dilute solution. The transmission electron micrographs revealed the presence of closed vesicles and twisted ribbons in the aqueous solutions of the amphiphiles. Optical microscopic images also showed the existence of twisted ribbons and rope-like helical structures in the case of SAUV.

The spontaneous self-assembly of molecules into supramolecular architectures is a result of various noncovalent interactions such as hydrophobic, hydrogen-bonding, electrostatic, dipole–dipole, and van der Waals interactions. The hydrophobic interaction between long hydrocarbon chains of amphiphilic molecules is essential in the formation of supramolecular aggregates. The geometrical characteristics of surfactant molecules determine the type of self-assembly structure taken in solution. Depending upon the packing parameter, the surfactant can self-assemble to form spherical, rod-like micelles, bilayers, vesicles/liposomes, lamellar structures, and so forth in solution.[1] It has been found that a change in the headgroup and the hydrocarbon tail affects the morphology of the self-assemblies. Vesicles are usually formed by double-chain surfactants. However, recent reports have shown that vesicles are also formed from single-tailed amphiphiles.[2,3] In fact, some fatty acid soaps form vesicles upon partial protonation.[4–6] On the other hand, introduction of electric charges can increase the average curvature, facilitating formation of vesicles from the lamellar phase.[7,8] In addition, short-range attractive interactions such as hydrogen bonding can also be a driving force in the formation of bilayer self-assemblies.[9–13] For example, hydrogen-bonding interaction between the protonated and nonprotonated headgroups of amine oxides[9] and fatty acid soaps,[4–6] and amide hydrogen bonding in *N*-acylamino acid surfactants (NAAS)[14–19] have been proposed to explain the mechanism of vesicle formation.

Recently, optically active NAAS have attracted considerable attention because of their chirality, which is an important phenomenon in nature.[17a,20] Further, NAAS are currently used as detergents, foaming agents, and shampoos as they are mild, nonirritating to human skin, and easily biodegradable.[21] They have also been shown to be useful in stereoselective synthesis.[22] One of the most important properties of these supramolecular assemblies is chiral recognition. The chiral recognition properties of the monolayers of NAAS have recently been reported.[20] On the other hand, the chiral discrimination by these surfactants in solution has been exploited by separation scientists.[23,24] NAAS are a class of surfactants that show interesting aggregation properties in solution. NAAS have been reported to self-organize in water[15–18,20a] and also in organic solvents[13,14,25] to form various types of supramolecular structures. These supramolecular assemblies generate bilayers in water with shapes like planar membranes, tubules, helices, ribbons, and rods. It has been demonstrated that the chirality of amphiphilic molecules imparts stability to the hydrophobic aggregates.

In this work, we investigate the aggregation behavior of sodium *N*-(11-acrylamidoundecanoyl)-L-valinate (SAUV) and -L-threoninate (SAUT) (see Chart 1 for structures). The surface and interfacial properties of the surfactants have also been compared. Fluorescence probe methods have been used to characterize the self-assemblies. The mean size of the self-assemblies has been measured by the dynamic light scattering

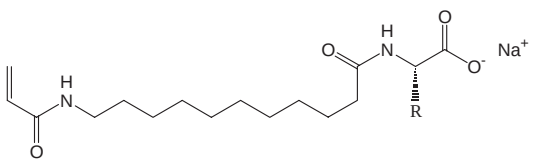

R = $CH(CH_3)_2$, **SAUV**
R = $CH(CH_3)OH$, **SAUT**

Chart 1. General chemical structure of SAUV and SAUT.

Published on the web January 13, 2006; DOI 10.1246/bcsj.79.59

technique. The circular dichroism spectra of SAUV and SAUT have been recorded to examine formation of chiral self-assemblies. We have also taken transmission electron microscopic and light microscopic images to visualize the shape of the self-assemblies. The hydrogen-bonding interactions between hydrophobic tails having an acrylamido group at the end of the acyl chain and between the polar headgroups have been shown to have a profound effect on the formation of the self-assemblies.

Experimental

Materials. The fluorescence probes pyrene and 1,6-diphenyl-1,3,5-hexatriene (Aldrich) were recrystallized from an acetone–ethanol mixture at least three times. The purity of the compounds was tested by fluorescence emission and excitation spectra. Acryloyl chloride and 11-aminoundecanoic acid (Aldrich), *N*-hydroxysuccinimide, dicyclohexylcarbodiimide, L-threonine, and L-valine (SRL) were used without further purification. Analytical grade sodium hydroxide, sodium hydrogencarbonate, sodium dihydrogenphosphate, disodium hydrogenphosphate, sodium acetate, sodium chloride, and hydrochloric acid were procured locally and were used directly from the bottle.

Synthesis. *N*-(11-Acrylamidoundecanoyl)-L-valine (AUV) and -L-threonine (AUT) were synthesized from *N*-hydroxysuccinimide ester of 11-acrylamidoundecanoic acid (AUA) and L-valine or L-threonine by slight modifications of the method reported in the literature.[26] AUA was synthesized and purified according to a procedure described elsewhere.[27] The molecular structures of the compounds were confirmed by elemental analysis, ^{1}H NMR, and FT-IR spectra.

***N*-(11-Acrylamidoundecanoyl)-L-valine:** Melting point: 80–82 °C; $[\alpha]_D^{25}$ (0.5%, CH_3OH) = −6.6°; FT-IR spectra (KBr, cm^{-1}): 3312 (N–H stretching), 2932 (alkyl C–H stretching), 1652 (amide-I band), 1624 (H_2C=CH– stretching), 1559 (amide-II band); ^{1}H NMR (200 MHz, $CDCl_3$): δ (δ in ppm, J in Hz): 6.24 (dd, 1H, J_{trans} = 17.27, J_{gem} = 1.736, H*H*C=CH), 6.1 (dd, 1H, J_{cis} = 9.83, J_{trans} = 17.27, H_2C=C*H*), 5.67 (dd, 1H, J_{gem} = 1.736, J_{cis} = 9.83, *H*HC=CH), 4.57 (dd, 1H, J = 3.92, 6.76, –NH–C*H*–COOH), 3.36–3.26 (m, 2H, CH_2=CH–CONH–CH_2), 2.16 (t, 2H, J = 7.2, –CH_2–CH_2–CONH–), 1.97–1.82 (m, 1H, –C*H*(CH_3)$_2$), 1.64–1.41 (m, 4H, –CH_2–(CH_2)$_6$–CH_2–), 1.26 (brs, 12H, –CH_2–(CH_2)$_6$–CH_2–), 0.76–0.74 (d, 3H, J = 2.99, –CH(CH_3)(CH_3)), 0.73–0.71 (d, 3H, J = 2.98, –CH(CH_3)(CH_3)); Anal. Calcd for $C_{19}H_{34}O_4N_2$: C, 64.38; H, 9.67; N, 7.90%. Found: C, 64.61; H, 9.64; N, 7.69%.

***N*-(11-Acrylamidoundecanoyl)-L-threonine:** Melting point: 74–76 °C; $[\alpha]_D^{25}$ (0.5%, CH_3OH) = −3.6°; FT-IR spectra of (KBr, cm^{-1}): 3313 (N–H stretching), 2927 (alkyl C–H stretching), 1661 (amide-I band), 1635 (H_2C=CH– stretching), 1544 (amide-II band); ^{1}H NMR (200 MHz, $CDCl_3$ + DMSO-d_6): δ (δ in ppm, J in Hz): 7.02 (brs, 1H, CH_2=CH–CON*H*), 6.68 (d, 1H, J = 8.98, –CON*H*–CHCH(CH_3)OH), 6.00 (dd, 1H, J_{gem} = 1.89, J_{trans} = 16.8, H*H*C=CH), 5.29 (dd, 1H, J_{gem} = 1.89, J_{cis} = 9.86, *H*HC=CH), 4.19–4.13 (dd, 1H, J = 2.69, 6.28, –CONH–C*H*CH(CH_3)-OH), 3.27–3.15 (m, 1H, –CHC*H*(CH_3)OH), 3.0–2.89 (m, 2H, CH_2=CH–CONH–CH_2), 1.99 (t, 2H, J = 7.25, –CH_2–CH_2–CONH–), 1.58–1.5 (d, 3H, J = 6.02, –CH(CH_3)OH), 1.50–1.28 (m, 4H, –CH_2–(CH_2)$_6$–CH_2–), 1.05 (brs, 12H, –CH_2–(CH_2)$_6$–CH_2–), 0.88 (d, 2H, J = 6.3, –CH(C$H_2$$CH_2$OH)COOH); Anal. Calcd for $C_{18}H_{32}O_5N_2$: C, 60.66; H, 9.04; N, 7.86%. Found: C, 60.55; H, 9.05; N, 8.02%.

The sodium salts were prepared by stirring the respective acid in a water–tetrahydrofuran mixture containing equimolar sodium hydrogencarbonate for 18 h. The salt was obtained as a solid mass after evaporation of the solvent. The crude salt was recrystallized twice from a petroleum ether–ethanol mixture.

Methods. General Instrumentation: The ^{1}H NMR spectra were recorded on a Bruker SEM 200 instrument in $CDCl_3$ solvent using TMS as the standard. The UV–visible spectra were recorded on a Shimadzu (model 1601) spectrophotometer. The optical rotation was measured with a Jasco P-1020 digital polarimeter. The CD spectra were recorded on a Jasco J-810 spectropolarimeter using quartz cells of 2 or 10 mm path length. The surface tension measurements were performed with a Torsion Balance (Hardson & Co., Kolkata) using the Du Nuoy ring detachment method. Conductivity measurements were performed by use of a digital Thermo Orion (model 150A+) conductivity meter, which uses a cell constant equal to 0.467 cm^{-1}. All measurements were carried out at room temperature (~30 °C) unless otherwise mentioned.

Fluorescence Measurements: The steady-state fluorescence spectra were measured on a SPEX Fluorolog-3 spectrophotometer. A saturated solution of pyrene ($C = 3.9 \times 10^{-7}$ M) was made in Milli-Q water. The pyrene solutions were excited at 335 nm and their emission intensities were measured as the area under the curve in the wavelength range of 350 to 500 nm. Each spectrum was blank subtracted and was corrected for lamp intensity variations during measurement. The excitation and emission slit widths were both set to 1 nm. Each measurement was repeated at least three times and the mean value was recorded.

Steady-state fluorescence anisotropy (r) was measured on a Perkin-Elmer LS-55 luminescence spectrometer equipped with filter polarizers that use the L-format configuration. The temperature of the water-jacketed cell holder was controlled by use of a Thermo Neslab (RTE 7) circulating bath. Since DPH is insoluble in water, a 2 mM stock solution of the probe in a 20% (v/v) methanol–water mixture was prepared. The final concentration of the probe was adjusted to 2 μM by the addition of the appropriate amount of the stock solution. The sample was excited at 350 nm and the emission intensity followed at 450 nm. The excitation and emission slit widths were 2.5 and 5 nm, respectively. The emissions were detected through a cutoff filter for wavelengths below 390 nm. The r-value was calculated from

$$r = (I_{VV} - GI_{VH})/(I_{VV} + 2GI_{VH}), \quad (1)$$

where I_{VV} and I_{VH} are the fluorescence intensities polarized parallel and perpendicular to the excitation light, and G is the instrumental grating factor ($G = I_{VV}/I_{VH}$).

Laser Light Scattering: The laser light scattering (LLS) measurements were performed with a Photal DLS-7000 (Otsuka Electronics Co., Ltd., Osaka, Japan) optical system equipped with an Ar^+ ion laser (75 mW) operated at 16 mW at λ_o = 488 nm. A 10 mM solution of the amphiphile was prepared in Milli-Q water. The solution was filtered directly into the scattering cell through a Millipore Millex syringe filter (Triton free, 0.22 μm). The LLS measurements started 5–10 min after the sample solutions were placed in the LLS optical system to allow the sample to equilibrate at the bath temperature. For all light scattering measurements, the temperature was 25 ± 0.5 °C. The scattering intensity was measured at various angles (30–135°) to the incident beam. Data acquisition was carried out for 10 min, and each experiment was repeated two or three times. In dilute solutions of monodisperse particles, the time decay of the autocorrelation function of the concentration fluctuations $g^{(1)}(q,t)$ is a single exponential with a characteristic decay rate (Γ). Γ is proportional

to q^2 ($\Gamma = Dq^2$), which characterizes a translational diffusion with the mutual diffusion constant D. The scattering vector, q, is given by the equation

$$q = 4\pi n/\lambda_o \sin(\theta/2), \quad (2)$$

where n is the refractive index of the solvent and θ is the scattering angle. The mutual diffusion constant is related to the average hydrodynamic radius R_h of the particles through the equation

$$D = kT/6\pi\eta R_h = \Gamma/q^2, \quad (3)$$

where k is the Boltzmann constant, η is the solvent viscosity, and T is the absolute temperature. For data analysis, we adopted the classical cumulant method.[28]

Microscopy: The transmission electron microscopic (TEM) measurements were performed using a 5 mM solution of the amphiphiles after equilibration for 2–3 h. A carbon-coated copper grid was immersed in a drop of aqueous solution of the amphiphile for 1 min, blotted with filter paper, and then negatively stained with freshly prepared 1.0% aqueous uranyl acetate. The specimens were air-dried for 1 h and then examined on a Phillips CM 200 Electron Microscope operating at an accelerating voltage of 200 keV at room temperature. For light micrographs, a drop of the appropriate solution was placed on a thoroughly cleaned glass plate. The light micrographs were obtained from Leica-DMRXP microscope.

Results and Discussion

Surface Tension Studies. Surface tension measurements were performed to determine the critical aggregation concentration (*cac*). The surface tension method is the most versatile among all of the methods that are used to estimate *cac*. This is not only because *cac* can be obtained from a plot of surface tension (γ) versus log(concentration), but also because one can get information regarding the adsorbed layer of surfactant molecules at the air/water interface. The plots of γ vs $\log C$ for the aqueous solutions (pH = 8) of the amphiphiles are shown in Fig. 1. The *cac* values of the amphiphiles were determined from the break point of the respective plots. It is interesting to note that there are two breakpoints in both of the plots. The second break may be associated with the onset of secondary aggregation of the surfactant. Such types of post micellar aggregation have also been reported for various synthetic surfactant systems.[29–31] In fact, three transition points (the cmc, micellar growth, and micellar entanglement) observed for many ionic surfactants have been reported in the literature.[32,33] It should be noted here that sodium 11-acrylamidoundecanoate (SAU) has only one *cac* (0.4 mM).[19] Therefore, it appears that the post micellar aggregation must be induced by the amide linkage near the surfactant headgroup. The *cac* and γ_{cac} values of the amphiphiles are listed in Table 1. The γ_{cac} values indicate that both amphiphiles are weakly surface-active. It can be observed that the first *cac* of SAUT is less than that of SAUV, but the order of the second *cac* values is reversed. This may be due to the difference in polarity of the amino acid side chains.

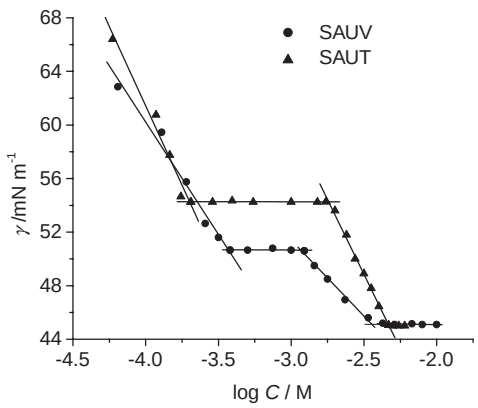

Fig. 1. Plots of surface tension (γ) vs $\log C$ of SAUV and SAUT in water.

Interfacial Properties. The surface tension measurements also allow one to determine the surface area per surfactant molecule at the interface, which can be calculated from the slope of the linear part using the equations[34]

$$\Gamma_2 = -1/nRT(d\gamma/d\ln C), \quad (4)$$

$$a_o = 10^{18}/(\Gamma_2 N_A), \quad (5)$$

where Γ_2 is the maximum surface excess concentration expressed in mol m^{-2}, a_o is the minimum surface area (in nm^2) per surfactant molecule at the air/water interface, γ is surface tension in mN m^{-1}, N_A is the Avogadro number, $R = 8.314$ J mol^{-1} K^{-1}, and $n = 2$ for dilute solutions of 1:1 ionic surfactants.[34] The Γ_2 and a_o values of the surfactants thus obtained are listed in Table 1. For both surfactants, the a_o value is ~1.0 nm^2, which is indicative of the formation of bilayer aggregates.[30]

The standard free energy of adsorption (ΔG°_{ad}) of the surfactants at the air–water interface can be evaluated by use of the equation[35]

$$\Delta G^\circ_{ad} = \Delta G^\circ_a - \pi_{cac}/\Gamma_2, \quad (6)$$

where π_{cac} is the surface pressure ($=\gamma_o - \gamma_{cac}$, γ_o is the surface tension of pure water), and ΔG°_a is the standard free energy of aggregation per mole of surfactant molecule. ΔG°_a can be obtained by using the equation[36]

Table 1. Surface, Interfacial, and Self-Assembly Properties of SAUV and SAUT in Aqueous Solutions at 303 K

Properties	SAUV	SAUT
cac/mM	0.35, 0.21[a)]	0.20, 0.31[a)]
cvc/mM	3.36, 3.13[a)]	4.09, 4.90[a)]
γ_{cac}/mN m^{-1}	50.6	54.3
π_{cac}/mN m^{-1}	20.6	16.9
α	0.83	0.83
$\Gamma_2 \times 10^6$/mol m^{-2}	1.70	2.09
a_o/nm^2 molecule^{-1}	0.98	0.80
ΔG°_a/kJ mol^{-1}	−23.4	−25.1
ΔG°_{ad}/kJ mol^{-1}	−35.5	−33.2
$D \times 10^{12}$/m^2 s^{-1}	4.44	4.66
R_h/nm	54.6	55.0
$N_{agg} \times 10^{-4}$	7.65	9.50
I_1/I_3	1.68 (1.30)	1.76 (1.40)
r	0.20	0.19
T_c/K	313	317
pK_a	6.80	6.50

a) Data obtained from fluorescence measurement; values within the parenthesis represent corresponding quantity above *cvc*.

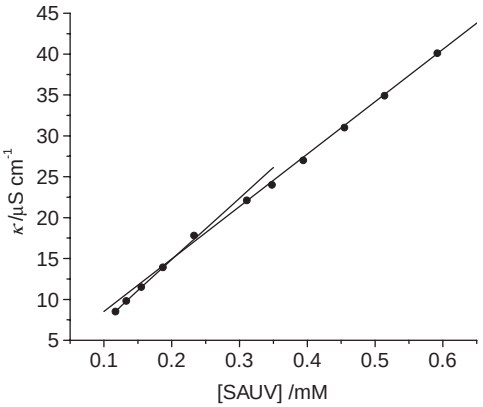

Fig. 2. Plots of κ versus SAUV concentration.

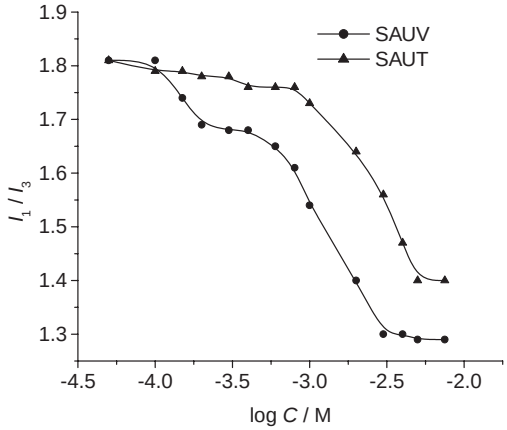

Fig. 3. Plots of I_1/I_3 versus $\log C$ of SAUV and SAUT.

$$\Delta G^{\circ}_{a} = (2-\alpha)RT\ln(cac/C_r), \quad (7)$$

where α is the degree of counterion dissociation, and C_r ($=1\,\mathrm{mol\,L^{-1}}$) is the reference concentration. The α-value for SAUV was obtained from the ratio (S_2/S_1) of the slopes of the straight lines in the post- and premicellar concentration range in the plot of conductivity (κ) vs concentration (Fig. 2). Since the chemical structures of the surfactants are similar they are expected to have similar α-values. Therefore, the α-value for SAUT was taken to be equal to that of SAUV. The α-value along with the ΔG°_{a} and ΔG°_{ad} values are listed in Table 1. It can be found that the ΔG°_{a} for SAUT is slightly more negative in comparison to that of SAUV. This means that aggregation is more favorable in the case of SAUT. This is consistent with the lower *cac* of SAUT compared to that of SAUV. This must be due to the more polar amino acid side chain of SAUT. The π_{cac} value of SAUT is less than that of SAUV, which means that the surface adsorptivity of the former surfactant is less than that of the latter. This is indicated by the slightly less negative ΔG°_{ad} value of SAUT. This is due to the increased polarity of the amino acid side chain in the SAUT surfactant compared to that in SAUV. In fact, Miyagishi and co-workers have also reported a progressive increase in the π_{cac} value of NAAS with the increase in hydrophobicity of the amino acid side chain.[37]

Micropolarity of the Hydrophobic Domains. The apparent micropolarity of the aggregates was estimated by measuring the intensity ratio I_1/I_3 of the first (372 nm) and the third (384 nm) vibronic peaks of the pyrene fluorescence spectrum. The polarity ratio was measured in the presence of different concentrations of SAUV and SAUT. The representative plots of I_1/I_3 as a function of surfactant concentration are shown in Fig. 3. The plots show a fall of the I_1/I_3 ratio, which indicates that the pyrene probe moves from a high polarity region to low polarity.[38] Also, a clear two-step change of the I_1/I_3 value with an increase in surfactant concentration is evident from the plots. This is consistent with the two breaks in the surface tension plot (Fig. 1). The polarity ratios for both types of aggregates are included in Table 1. For both surfactants, the polarity ratio corresponding to the first step is not very different from that of water (1.81). This indicates that the probe molecule is solubilized within nonspherical aggregates and is partially exposed to solvent molecules. This may suggest formation of either small micellar aggregates or flat bilayer structures. The possibility of formation of small premicellar aggregates, however, can be ruled out on the basis of the a_o value and the fluorescence anisotropy (r) value of the DPH probe as discussed in the following section. It is interesting to note that the micropolarity of the secondary aggregates of SAUV or SAUT is much lower compared to that of bilayer structures. The I_1/I_3 ratio for the secondary aggregates of SAUV is less than that of SAUT. This suggests more ordering at the interface and formation of spherical aggregates. The ordering of the aggregate interface reduces the degree of water penetration in the hydrocarbon layer, which is in accordance with the reduction observed in micropolarity sensed by the probe molecules. Therefore, it can be concluded that at concentrations above the second *cac* both surfactants form closed vesicles in water. Therefore, the second *cac* value can be interpreted as the critical vesicle concentration (*cvc*).

Microfluidity of Hydrophobic Domains. The fluorescence anisotropy (r) measurement can provide useful insights into the physical properties of lipid bilayers. The r can be taken as an index of microfluidity of the vesicle lipidic core. The DPH is a well-known membrane fluidity probe and has been used for studying many lipid bilayer membranes.[39–41] Therefore, the steady-state fluorescence anisotropy of the DPH probe was measured as a function of concentration above the *cac* of SAUV and SAUT. The anisotropy is relatively high at concentrations above the *cac*, which remained unchanged upon increases of surfactant concentration. That is, the microenvironments of the DPH probe in both types of aggregates are similar. Thus, it rules out transformation of the bilayer structures to micellar aggregates. The high r-value at a surfactant concentration just above the *cac* also excludes formation of any micellar structures, as the DPH probe in the latter type of aggregates usually has low r-values. The steady-state fluorescence anisotropy of DPH measured in a 5 mM surfactant solution at room temperature are listed in Table 1. The r-values are found to be greater than that of lecithin liposomes ($r \sim 0.098$), but less than that of sphingomyelin liposomes ($r \sim 0.247$).[40] The relatively high value of r suggests an ordered environment around the DPH probe in the assemblies. This might be due to the intermolecular amide hydrogen bonding between two surfactant molecules. The hydroxy group of the amino acid side

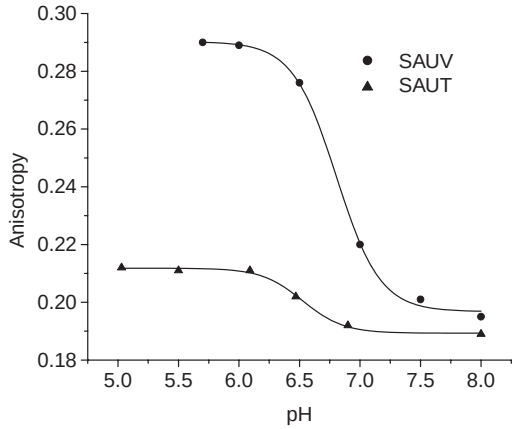

Fig. 4. pH-Dependence of fluorescence anisotropy of DPH in the presence of 2 mM SAUV and SAUT.

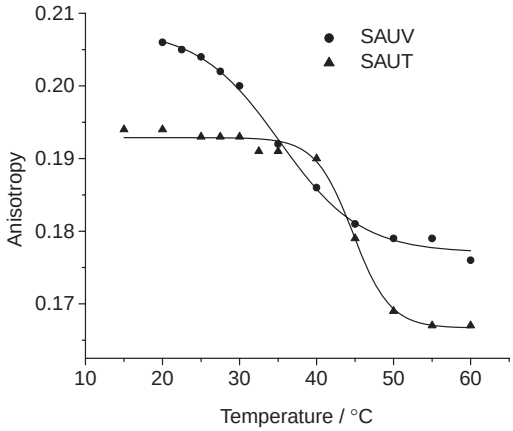

Fig. 5. Plots of the temperature-dependence of the fluorescence anisotropy of DPH in 5 mM SAUV and SAUT surfactant solutions.

chain in SAUT can also participate in intermolecular hydrogen bonding, making the packing of the hydrophobic chains very tight. The high microviscosity and low micropolarity of the self-assemblies clearly suggest the existence of liposome-like membrane structures in dilute solutions of the amphiphiles.

pH-Dependence of Bilayer Self-Assemblies. The fluorescence anisotropy of the DPH probe in the presence of the surfactants was also found to increase with a decrease in the pH of the solution. Figure 4 shows the variations of anisotropy as a function of pH for 2 mM SAUV and SAUT. Similar but small changes were also observed with 10 mM surfactant solutions. The sigmoid change of the anisotropy value for both amphiphiles suggests a two-state process. This may be due to protonation of the COO^- group that reduces ionic repulsions as well as promotes intermolecular hydrogen bonding between the COOH and COO^-, or between COOH and CONH groups at the interface. The ordering of the self-assemblies at the interface should also result in compact packing in the interior of the bilayer aggregates as manifested by the increase of anisotropy. The inflection point of the plots in Fig. 4 can be taken as the pK_a of the respective amphiphile. Thus, pK_a values of the corresponding acid forms of SAUV and SAUT are 6.8 and 6.5, respectively. The pK_a values obtained from the inflection points are higher than the pK_a values of the corresponding fatty acids.[42] The increase of pK_a may be attributed to the high charge densities on the bilayer surface. A similar increase of pK_a has also been suggested for fatty acids by other researchers.[43] Thus, it can be concluded that bilayer self-assemblies are more favored at a pH equal to the respective pK_a value, which corresponds to when the COO^- groups are half protonated. The pH adjustment provides a way for the bilayer surface charge density to be varied precisely through changing the degree of protonation of the amino acid headgroup. As a result, the concomitant electrostatic and hydrogen-bonding interactions may force the bilayers to adopt a spherical shape to form closed vesicles.

Phase Transition of the Bilayer Self-Assemblies. The phase transitions of membranes are also revealed by the fluorescence anisotropy of DPH. In order to determine the phase-transition temperature, we have studied the temperature effect on the fluorescence anisotropy of DPH in a 5.0 mM surfactant solution. The plot of the variation of r as a function of temperature is shown in Fig. 5. The large change in anisotropy with an increase in temperature can be associated with the phase transition between the gel-like states to the liquid crystalline state. Thus, the temperature corresponding to the inflection point can be taken as the phase-transition temperature, T_c. The results are included in Table 1. The phase-transition temperature in the case of SAUT vesicles is higher than that of SAUV vesicles. This may be due to the stronger intermolecular hydrogen bonding involving the OH group of the amino acid side chain that strengthens the bilayer membrane structure.

Effect of Intermolecular Hydrogen Bonding. It can be shown that the binding forces for the stability of bilayer structures are generated mainly from noncovalent interactions such as hydrogen bonding. The molecular structures (see Chart 1) of the amphiphiles show that there can be two stable intermolecular hydrogen bonds. In one of our recent publications, we have shown intermolecular hydrogen bonding between the secondary amide groups at the end of the hydrocarbon tails of SAU.[19] The influence of the amide linkage at the hydrophilic headgroup on the aggregation properties of NAAS has already been established in the literature.[9] The multiple hydrogen bonds between N–H and C=O groups assist the surfactant molecules to self-assemble to form a parallel arrangement of the corresponding hydrophobic tails, such that the surfactant molecules can self-organize into bilayer structures in water. The low *cac* of the amphiphiles and the large size of the aggregates compared to that of the corresponding fatty acid salts[44] suggest that the intermolecular hydrogen-bonding interaction between amide groups enhances the hydrophobic interaction that leads to tight packing of the hydrocarbon chains. This is manifested by the low micropolarity and high microviscosity of the vesicles, as discussed above. However, the bilayer sheets with strong surface binding interactions may also tend to form spherical vesicles, ribbons, mono or multilayer tubules, and rodlike micelles. Undeniably, the presence of vesicles is evident from the TEM images of the dilute solutions of the amphiphiles.

Circular Dichroism Spectra. The bilayer sheets of SAUV and SAUT can get twisted due to the presence of chiral center forming helical aggregates. The existence of chiral aggregates, e.g., twisted ribbons and helical strands in addition to spherical

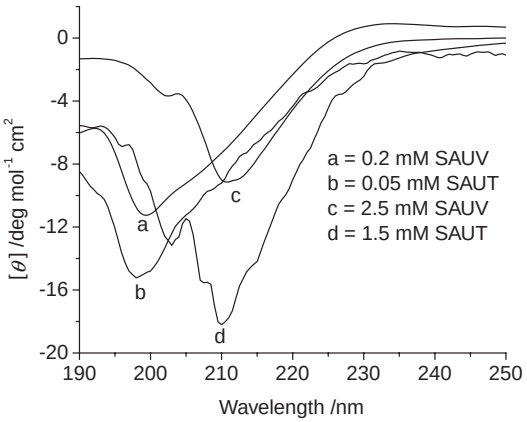

Fig. 6. Circular dichroism spectra of SAUV and SAUT in water: (a and b) (<*cac*), and (c and d) (>*cac*).

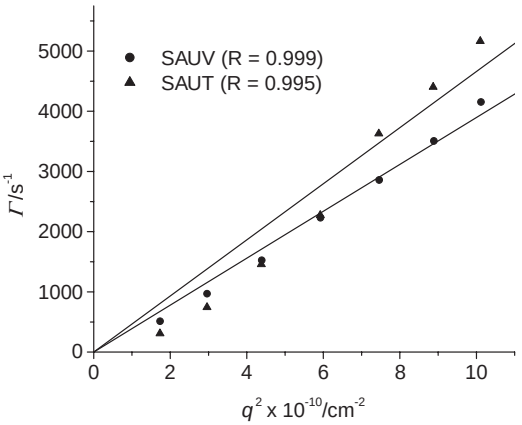

Fig. 7. Plots of relaxation time, Γ, of the self-assemblies in 5 mM solution of SAUV and SAUT as a function of the square of the scattering vector, q^2.

vesicles and tubules, has been reported in the case of optically active NAAS by others.[15–18,20–22,25] Homochiral interactions between the chiral groups have been proposed to account for the twisting that forms the helices.[45] Formation of chiral helical aggregates is normally manifested in the CD spectra and has been demonstrated by many authors.[45–47] Therefore, aqueous solutions of SAUV and SAUT were examined for chiral organization by CD spectroscopy. The CD spectra recorded in aqueous solutions of the amphiphiles at concentrations above and below the respective *cac* are shown in Fig. 6. The CD spectra of both SAUV and SAUT in water above *cac* show a negative band at 212 nm. In aqueous solutions of SAUV or SAUT at concentrations below *cac*, the peak at 212 nm disappears and a new peak at 200 nm appears. The disappearance of the CD band at 212 nm below *cac* indicates formation of chiral structures through aggregation. The appearance of a similar CD band at ~212 nm in alcoholic solutions of optically active *N*-lauroyl-L-valine has also been reported.[48] The CD peak at 212 nm could be associated with the $\pi \rightarrow \pi^*$ transition of the amide bond.[48–50] The CD spectra are similar to those of *N*-palmitoyl- or *N*-stearoyl-L-serine amphiphile in water.[45] This unique spectral feature, as suggested by Shinitzky et al., is due to a network of the amide bonds with distinct chiral features.[14] The CD spectra seems to have originated from a repetitive arrangement of the amide bond planes on the surface of the bilayer assemblies.

Laser Light Scattering Studies. LLS measurements were performed to obtain mean aggregate sizes. The average translational diffusion coefficients (D) of the aggregates were obtained from the slope of the plot of the relaxation rates versus square of the scattering vector, q^2 (Fig. 7). The plots are linear and pass through the origin, suggesting that the apparent diffusion coefficient is due to Brownian motion of the particles. The angular dependence of the apparent diffusion constant suggests that the aggregates are polydispersed in size. The apparent D values of the aggregates formed by the amphiphiles are listed in Table 1. The D values of the amphiphiles are of the order of 10^{-12} m^2 s^{-1}, which is much smaller than that of normal spherical micelles (~10^{-10} m^2 s^{-1}).[31] The R_h values of the amphiphiles are listed in Table 1. The size of the aggregates indicates that they are not micelles. Therefore, as indicated by surface tension and fluorescence probe studies, the large aggregates must be vesicles. The data suggest that the vesicles of both SAUV and SAUT are similar in size. Assuming unilamellar vesicles, the R_h values can be used to calculate the mean aggregation number of the vesicles formed by the amphiphiles by use of equation

$$N_{agg} = 8\pi {R_h}^2 / a_o. \quad (8)$$

The N_{agg} values at concentrations above the second *cac* of the respective amphiphiles are listed in Table 1. As expected, the N_{agg} values for both surfactants are very large. The existence of large vesicles is further substantiated by the results of microscopic studies. The vesicular solutions of neither surfactant showed any significant variation in R_h values or in static turbidity at room temperature for a period of more than a week. This suggests that the individual vesicles did not fuse to form clusters within this period.

Microscopic Images. To investigate the microstructure of the self-assemblies of SAUV and SAUT, TEM pictures were taken in aqueous surfactant solutions having concentrations below and above the *cvc*. No identifiable structures could be observed at concentrations below *cvc* for both surfactants. The TEM images of aqueous solutions (5 mM) of SAUV and SAUT are depicted in Figs. 8(A, B) and 8C, respectively. The TEM pictures clearly exhibit polydisperse spherical vesicular structures. The vesicles of SAUV have inner diameters in the range of 30–150 nm. On the other hand, the size of the vesicles of SAUT are much bigger (50–900 nm) than those of SAUV. However, in both cases the smaller vesicles are more in number. The sizes obtained are consistent with those obtained from LLS measurements. From the TEM pictures, it is not possible to comment on whether the vesicles are unilamellar of multilamellar. Micrograph 8B of SAUV, obtained by negatively staining with 2% phosphotungstic acid (after adjusting the pH to 8.0), also reveals the presence of twisted ribbons in solution. No other chiral aggregates were observed in the electron micrographs of SAUV or SAUT. This might be due to the inherent artifact of techniques that involve drying of the sample. However, the optical micrographs (Figs. 9A and 9B) of a solution of SAUV in water revealed tubules, twisted ribbons, and two-strand helices. In the optical micrographs of SAUT, we failed to identify such structures.

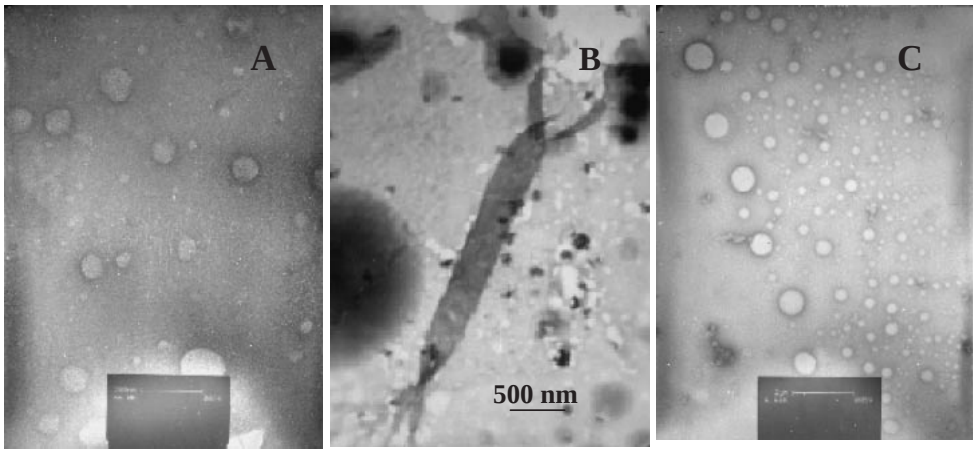

Fig. 8. Negatively stained TEM pictures for 5 mM solutions of SAUV (A and B) and SAUT (C).

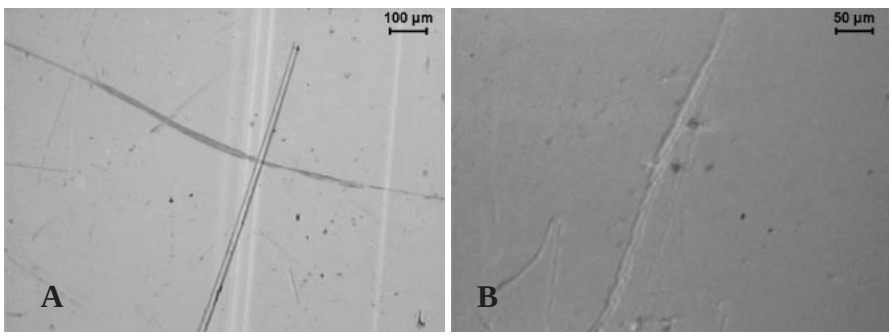

Fig. 9. Optical micrographs of 5 mM aqueous SAUV solution: tubules and twisted ribbon (A), and two-strand helix (B).

Concluding Remarks

The sodium *N*-(11-acrylamidoundecanoyl)-L-valinate, and -L-threoninate surfactants have two breakpoints in their surface tension plots. The first step corresponds to formation of flat bilayer structures and the second breakpoint is due to transformation of the bilayer structures to mainly closed vesicles. The amide hydrogen bonding near the surfactant headgroup is the driving force for secondary aggregation. Bilayer formation is more favored in the case of SAUT. Intermolecular amide hydrogen bonding between hydrophobic tails has been shown to be responsible for the formation of bilayer structures. The microenvironment of the self-assemblies is more nonpolar and viscous compared to that of normal micelles. The CD spectra of the amphiphiles indicated formation of chiral aggregates above the *cac*. The transmission electron micrographs revealed the presence of closed vesicles in aqueous solutions of the amphiphiles. The vesicles are stable for more than one week. The light micrographs showed the existence of tubules, twisted ribbons, and helical strands in the aqueous solution of SAUV.

This work was supported by CSIR (Grant No. 01(1664)/00/EMR-II) and DST (Grant No. SP/S1/G-36/99), New Delhi. S. Roy thanks CSIR for a research fellowship (9/81(380)/2002-EMR-I).

References

1 J. Israelachvili, *Intermolecular and Surface Forces with Application to Colloidal and Biological Systems*, Academic Press, London, **1985**.

2 A. Khan, E. F. Marques, *Curr. Opin. Colloid Interface Sci.* **2000**, *4*, 402.

3 J. F. B. N. Engberts, J. Kevelam, *Curr. Opin. Colloid Interface Sci.* **1996**, *1*, 779.

4 E. Bloechliger, M. Blocher, P. Walde, P. L. Luisi, *J. Phys. Chem. B* **1998**, *102*, 10383.

5 K. Edwards, M. Silvander, G. Karlsson, *Langmuir* **1995**, *11*, 2429.

6 J. M. Gebicki, M. Hicks, *Nature* **1973**, *243*, 232.

7 J. Oberdisse, C. Couve, J. Appell, J. F. Berret, C. Ligoure, G. Porte, *Langmuir* **1996**, *12*, 1212.

8 K. Edwards, J. Gustafsson, M. Almgren, G. Karlsson, *J. Colloid Interface Sci.* **1993**, *161*, 299.

9 H. Maeda, R. Kakehashi, *Adv. Colloid Interface Sci.* **2000**, *88*, 275.

10 H. Kawasaki, H. Maeda, *Langmuir* **2001**, *17*, 2278.

11 B. S. Li, J. Chen, C. F. Zhu, K. K. L. Leung, L. Wan, C. Bai, B. Z. Tang, *Langmuir* **2004**, *20*, 2515.

12 D. Kaneko, U. Olsson, K. Sakamoto, *Langmuir* **2002**, *18*, 4699.

13 S. Bhattacharya, Y. Krishnan-Ghosh, *J. Chem. Soc., Chem. Commun.* **2001**, 185.

14 M. Shinitzky, R. Haimovitz, *J. Am. Chem. Soc.* **1993**, *115*, 12545.

15 a) Y.-J. Zhang, M. Jin, R. Lu, Y. Song, L. Jiang, Y. Zhao, *J. Phys. Chem. B* **2002**, *106*, 1960. b) J.-H. Fuhrhop, C. Demoulin, J. Rosenberg, C. Boettcher, *J. Am. Chem. Soc.* **1990**, *112*, 2827.

16 a) C. Boettcher, B. Schade, J.-H. Fuhrhop, *Langmuir* **2001**, *17*, 873. b) J.-H. Fuhrhop, P. Schnieder, J. Rosenberg, E. Boekema, *J. Am. Chem. Soc.* **1989**, *109*, 3387.

17 a) S. Borocci, G. Mancini, G. Cerichelli, L. Luchetti, *Langmuir* **1999**, *15*, 2627. b) T. Imae, Y. Takahashi, H. Muramatsu, *J. Am. Chem. Soc.* **1992**, *114*, 3414.

18 a) D. Vollhardt, U. Gehlert, *J. Phys. Chem. B* **2002**, *106*, 4419. b) H. Kawasaki, M. Souda, S. Tanaka, N. Nemoto, G. Karlsson, M. Almgren, H. Maeda, *J. Phys. Chem. B* **2002**, *106*, 1524.

19 S. Roy, J. Dey, *Langmuir* **2003**, *19*, 9625.

20 a) X. Du, V. Hlady, *J. Phys. Chem. B* **2002**, *106*, 7295. b) X. Du, Y. Liang, *J. Phys. Chem. B* **2001**, *105*, 6092. c) X. Du, Y. Liang, *J. Phys. Chem. B* **2000**, *104*, 10047. d) S. Miyagishi, N. Takeuchi, T. Asakawa, M. Inoh, *Colloids Surf., A* **2002**, *197*, 125. e) J. Bella, S. Borocci, G. Mancini, *Langmuir* **1999**, *15*, 8025. f) F. Hoffmann, H. Huhnerfuss, K. J. Stine, *Langmuir* **1998**, *14*, 4525. g) D. P. Parazak, J. Y.-J. Uang, B. Turner, K. J. Stine, *Langmuir* **1994**, *10*, 3787.

21 a) M. Takehara, H. Moriyuki, I. Yoshimura, R. Yoshida, *J. Am. Oil Chem. Soc.* **1972**, *49*, 143. b) M. Takehara, *Colloids Surf.* **1989**, *38*, 149.

22 a) Y. Zhang, P. Sun, *Tetrahedron: Asymmetry* **1996**, *7*, 3055. b) M. Takeshita, H. Yanagihara, K. Terada, N. Akutsu, *Annu. Rep. Tohoku Coll. Pharm.* **1992**, *39*, 247. c) Y. Zhang, W. Wu, *Tetrahedron: Asymmetry* **1997**, *8*, 3575. d) M. J. Diego-Castro, H. C. Hailes, *Chem. Commun.* **1998**, 1549.

23 a) J. Clothier, S. Tomellini, *J. Chromatogr. A* **1996**, *723*, 179. b) P. Desbene, C. Fulchic, *J. Chromatogr. A* **1996**, *749*, 257. c) Y. Mechref, Z. El Rassi, *Chirality* **1996**, *8*, 518. d) S. Hara, A. Dobashi, Jpn. Kokai Tokkyo Koho 92 149,205, **1992**. e) S. Hara, A. Dobashi, Jpn. Kokai Tokkyo Koho 92 149,206, **1992**. f) D. Y. Chu, T. K. Thomas, *Macromolecules* **1991**, *24*, 2212. g) J. Wang, I. M. Warner, *Anal. Chem.* **1994**, *66*, 3773. h) H. H. Yarabe, S. A. Shamsi, I. M. Warner, *Anal. Chem.* **1999**, *71*, 3992. i) C. P. Palmer, *Electrophoresis* **2000**, *21*, 4054, and references therein.

24 a) C. P. Palmer, S. Terabe, *J. Microcolumn Sep.* **1996**, *8*, 115. b) C. P. Palmer, S. Terabe, *Anal. Chem.* **1997**, *69*, 1852. c) S. A. Shamsi, C. Akbey, I. M. Warner, *Anal. Chem.* **1998**, *70*, 3078. d) C. Akbey, I. M. Warner, S. A. Shamsi, *Electrophoresis* **1999**, *20*, 145. e) J. L. Hayenes, III, E. J. Billot, H. H. Yarabe, I. M. Warner, S. A. Shamsi, *Electrophoresis* **2000**, *21*, 1597.

25 a) J. Song, Q. Cheng, S. Kopta, R. C. Stevens, *J. Am. Chem. Soc.* **2001**, *123*, 3205. b) X. Luo, B. Liu, Y. Liang, *Chem. Commun.* **2001**, 1556.

26 Y. Lapidot, S. Rappoport, Y. Wolman, *J. Lipid Res.* **1967**, *8*, 142.

27 K. W. Yeoh, C. H. Chew, L. M. Gan, L. L. Koh, H. H. Teo, *J. Macromol. Sci., Chem.* **1989**, *26*, 663.

28 D. E. Koppel, *J. Chem. Phys.* **1972**, *57*, 4814.

29 a) B. Chu, Z. Zhou, *Physical Chemistry of Polyalkylene Block Copolymer Surfactants*, in *Nonionic Surfactants*, ed. by V. M. Nace, Surfactant Science Series, **1996**, Vol. 60, p. 67. b) S. Bhattacharya, J. Haldar, *Langmuir* **2004**, *20*, 7940.

30 a) Y.-Y. Won, A. K. Brannan, H. T. Davis, F. S. Bates, *J. Phys. Chem. B* **2002**, *106*, 3354. b) H. N. Ghosh, D. K. Palit, A. V. Sapre, K. V. S. Ramarao, J. P. Mittal, *Chem. Phys. Lett.* **1993**, *203*, 5.

31 a) P. A. Hassan, S. R. Raghavan, E. W. Kaler, *Langmuir* **2002**, *18*, 2543. b) C. Tanford, Y. Nozakk, M. F. Rohde, *J. Phys. Chem.* **1977**, *81*, 1555.

32 S. Miyagishi, H. Kurimoto, T. Asakawa, *Langmuir* **1995**, *11*, 2951.

33 a) S. Miyagishi, H. Kurimoto, T. Asakawa, *Bull. Chem. Soc. Jpn.* **1995**, *68*, 135. b) S. Miyagishi, H. Suzuki, T. Asakawa, *Langmuir* **1996**, *12*, 2900. c) S. Miyagishi, W. Akasofu, T. Hashimoto, T. Asakawa, *J. Colloid Interface Sci.* **1996**, *184*, 527.

34 M. J. Rosen, *Surfactants and Interfacial Phenomena*, 3rd ed., John Wiley & Sons, New York, **2004**, p. 60.

35 P. Mukherjee, *Adv. Colloid Interface Sci.* **1967**, *1*, 242.

36 S. P. Moulik, M. E. Haque, P. K. Jana, A. R. Das, *J. Phys. Chem.* **1996**, *100*, 701.

37 S. Miyagishi, T. Asakawa, M. Nishida, *J. Colloid Interface Sci.* **1989**, *131*, 68.

38 K. Kalyanasundaram, J. K. Thomas, *J. Am. Chem. Soc.* **1977**, *99*, 2039.

39 a) M. Shinitzky, Y. Barenholz, *J. Biol. Chem.* **1974**, *249*, 2652. b) J. R. Lakowicz, F. G. Prendergast, D. Hogen, *Biochemistry* **1979**, *18*, 508. c) F. G. Prendergast, R. P. Haugland, P. J. Callahan, *Biochemistry* **1981**, *20*, 7333. d) B. R. Lentz, *Chem. Phys. Lipids* **1993**, *64*, 99.

40 a) U. Cogan, M. Shinitzky, G. Weber, T. Nishida, *Biochemistry* **1973**, *12*, 521. b) K. A. Zachariasse, W. Kuhnle, A. Weller, *Chem. Phys. Lett.* **1980**, *73*, 6.

41 J. R. Lakowicz, *Principles of Fluorescence Spectroscopy*, Plenum Press, New York, **1983**, p. 132.

42 M. Ptak, M. Egret-Charlier, A. Sanson, O. Bouloussa, *Biochim. Biophys. Acta* **1980**, *600*, 387.

43 a) J. M. Gebicki, M. Hicks, *Chem. Phys. Lipids* **1976**, *16*, 142. b) D. P. Cisola, J. A. Hamilton, D. Jackson, D. M. Small, *Biochemistry* **1988**, *27*, 1881. c) D. P. Cisola, D. M. Small, *J. Am. Chem. Soc.* **1990**, *112*, 3214. d) T. H. Haines, *Proc. Natl. Acad. Sci., U.S.A.* **1983**, *80*, 160. e) W. Li, T. H. Haines, *Biochemistry* **1986**, *25*, 7477.

44 a) P. Walde, R. Wick, M. Fresta, A. Mangone, P. L. Luisi, *J. Am. Chem. Soc.* **1994**, *116*, 11649. b) P. A. Bachmann, P. L. Luisi, J. Lang, *Nature* **1992**, *357*, 57.

45 a) T. Kunitake, N. Nakashima, M. Shimomura, Y. Okahata, K. Kano, T. Ogawa, *J. Am. Chem. Soc.* **1980**, *102*, 6642. b) T. Kunitake, N. Nakashima, K. Morimitsu, *Chem. Lett.* **1980**, 1347.

46 K. Sakamoto, M. Hatano, *Bull. Chem. Soc. Jpn.* **1980**, *53*, 339.

47 a) K. Sakamoto, R. Yoshida, M. Hatano, *Chem. Lett.* **1976**, 1401. b) K. Sakamoto, R. Yoshida, M. Hatano, T. Tachibana, *J. Am. Chem. Soc.* **1978**, *100*, 6898.

48 W. B. Gratzer, G. M. Holzwarth, P. Doty, *Proc. Natl. Acad. Sci. U.S.A.* **1961**, *47*, 1785.

49 W. Moffitt, *J. Chem. Phys.* **1956**, *25*, 467.

50 K. Rosenheck, B. Sommer, *J. Chem. Phys.* **1967**, *46*, 532.